Northumbria Research Link

Northumbria
University
NEWCASTLE

University**Library**

Controlled Cooperative Wetting Enabled Heterogeneous Structured 3D Morphing Transducers

Sreepathy Sridhar, Cong Wang, Jonathan G. Terry, Xue Chen, Ansu Sun, Zhenghong Li, Haibao Lv, Ben Bin Xu, and Yifan Li*

A unique microfluidics approach for functional hydrogel patterning with multilayered heterogeneous structures is presented. Prepolymer solution droplets with differentiated sodium acrylate concentrations are dispensed/printed in a wetting-controlled "two-parallel plate" (TPP, like a Hele-Shaw Cell) system. The gelation within the system enables hydrogel bilayer structures with reconfigurable 3D deformations driven by in-plane and through-thickness heterogeneity under stimuli-responsive mask-less swelling/deswelling. The cooperation between swelling mismatch of functional groups results in a higher complexity of 3D reconfiguration in responding to discrete levels of stimulation inputs. This facile patterning technology with an in-built ionic hierarchy can be scaled up/down with advanced transducing functionalities in various fields.

1. Introduction

Inspired by nature,[1–3] morphing soft materials responding to external stimulation (e.g., electrical, mechanical, and chemical) has proven to exhibit applicability in various fields,[4–9] but not restricted to flexible electronics,[10,11] 4D printing,[12,13] biomedical transducers,[14] and soft robotics.[15,16] One of the desirable developments is to make the morphing process programmable[17–22] and reversible[23,24] through structured soft functional materials, which enable effective shape configuration design according to the applications. As one of the popular candidates, hydrogels have

drawn more significant attentions due to their open network structures, and ability to generate large changes[25,26] (therefore high deformation) in volume responding to various external stimulation. For example, by creating through-thickness,[20] in-plane gradient,[27] or combining the two[28] in structuring dissimilar hydrogel functional layers and blocks, controllable deformation such as bending and folding can be achieved.

The through-thickness gradient approach typically employs a hydrogel bilayer structure where the swelling behavior remains dissimilar across the thickness.[8] The differential swelling leads to internal stress mismatch and influence out-of-plane 3D morphing configurations, resulting a single configuration at certain external conditions (e.g., temperature, ion concentration).[16] When external conditions are altered, a wider range of deformation magnitude and/or a reversed shape (e.g., bending towards opposite direction, "C" becomes "Ɔ") can be achieved, and more complicated configurations can be accomplished via advanced 2D shape patterning.[8,21,29] On the other hand, the in-plane gradient approach typically employs 2D heterogeneity via a single layer of patterned functional hydrogel on the same plane, resulting in a bistable status where the buckling could happen in either directions.[16] Combining the ideas from both through-thickness and in-plane gradient modes, through a controlled "preswelling" process that determines swelling direction, programmable complex deformations were demonstrated by the "site-specific" patterned hydrogel blocks.[17,27] The resultant shape-morphing structure generated due to in-plane elastic mismatch between nonswelling substrate and controlled swellable gel blocks was more or less fixed.[17,27] Moreover, such an approach always requires pairs of silhouetted/holed "preswelling masks" to assist and orchestrate the swelling command, in order to reconfigure the deformation patterns.[16,17] Also, once deformed, it will be difficult/impossible to apply the silhouetted/holed mask again to reconfigure the shape. For the required bilayer system, thickness uniformity is important due to its role in initiating the inherent stress distribution. For homogeneous hydrogel single-layer structures, patterned or not, this can be achieved by spin coating, or molding the prepolymer hydrogel (pre-gel) in a "two-parallel plate" (TPP, like a Hele-Shaw cell) configuration, followed by gelation processes.[8,30] Inspired by natural biostructures, a single layer of encoded heterogeneous hydrogel building blocks has been exploited to form hierarchical complex hydrogel architectures, using droplet microfluidics (DMF) surface wetting control to guide the gel formation.[31]

S. Sridhar, Dr. C. Wang, Dr. X. Chen, A. Sun, Prof. B. B. Xu, Dr. Y. Li
Mechanical and Construction Engineering
Faculty of Engineering and Environment
Northumbria University
Newcastle upon Tyne NE1 8ST, UK
E-mail: yifan.li@northumbria.ac.uk
Dr. J. G. Terry
School of Engineering
Institute for Integrated Micro and Nano Systems
University of Edinburgh
Edinburgh EH9 3JF, UK
Z. Li, Prof. H. Lv
Science and Technology on Advanced Composites in Special
Environments Laboratory
Harbin Institute of Technology
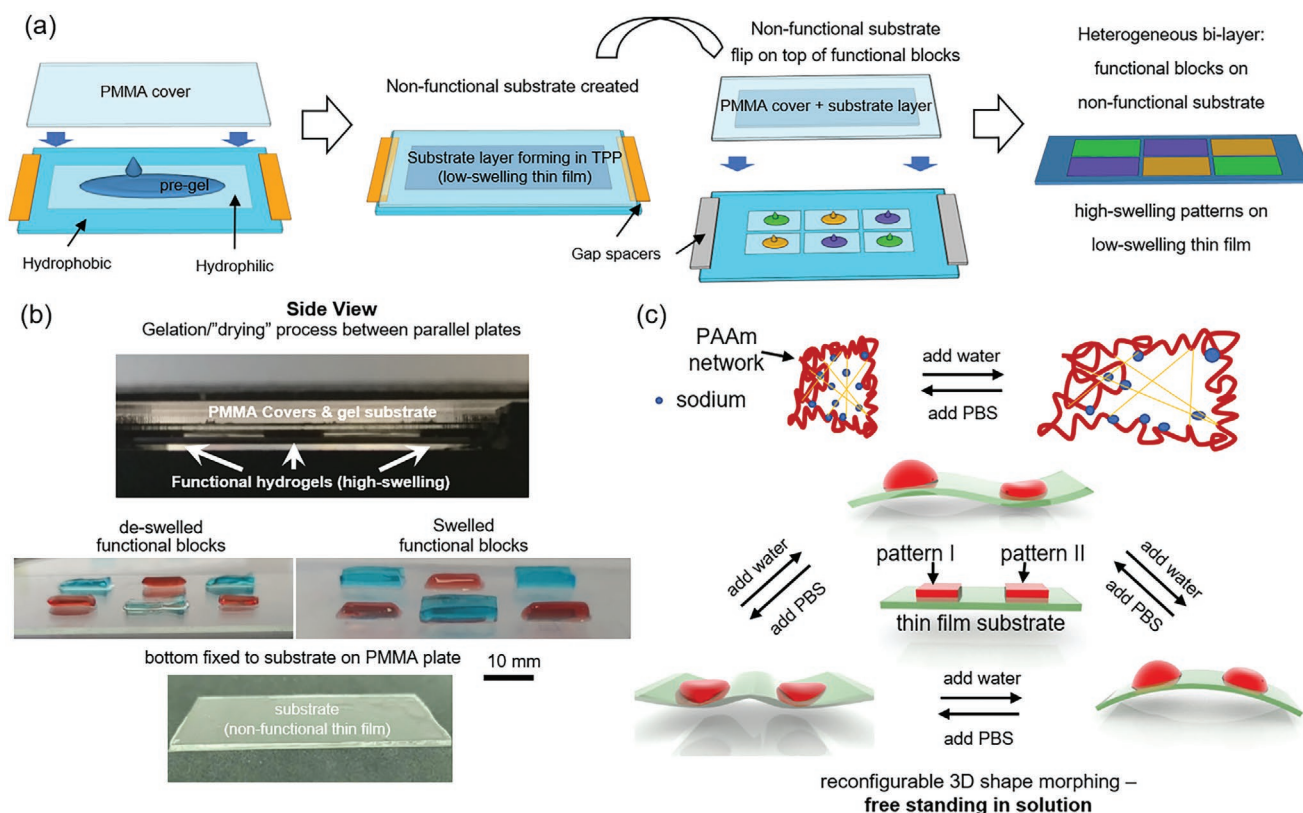Harbin 150080, P. R. China

Figure 1. Concept of the heterogeneous structured 3D morphing transducers: a) Bilayer hydrogel heterogeneous structure fabrication process, using droplet/open microfluidics in a TPP system with wetting control. b) Experimental photographs showing the side view of the gelation process in TPP, with dissimilar swelling behavior demonstrated on substrate fixed to a PMMA plate. c) Concept demonstration: multistate 3D shape reconfiguration guided by ionic environment using mask-less swelling/deswelling mechanism, (yellow lines in PAAm network represent cross-linker).

We hereby propose a facile approach to achieve not only programmable, but also reconfigurable maskless swelling/deswelling morphing structures that change shapes between various cooperative states responding to ionic strength (**Figure 1**). This reconfigurability was enabled by creating a heterogeneous nonfunctional/functional hydrogel bilayer, shaped and assembled in a TPP (like a Hele-Shaw cell) open-microfluidic configuration during gelation process, based on a setup we first revealed during.[32] The structure contains dissimilar high-swelling hydrogel blocks with mismatched swelling behavior, on top of a low-swelling (nonfunctional) substrate (Figure 1a). The resulted structure will respond to external ionic concentration, with both controllable deformation magnitude and shape reconfiguration (Figure 1b). Such development opens a range of future possibilities where combining "in-plane" 2D heterogeneity, complex patterns, and multilayer "though-thickness" structures will bring more advanced soft materials morphing control.

2. Results and Discussion

2.1. Reconfigurable 3D Morphing Transducers

The hierarchical patterned gels are prepared by two-step polymerization method, as shown in Figure 1a. A thin film nonfunctional substrate is polymerized to form polyacrylamide (PAAm) gels without the presence of sodium acrylate (SA). PAAm exhibits good biosafety characteristics towards human cells, which makes it a popular candidate in smart biomedical applications.[33] Alongside the nonfunctional substrate fabrication, a series of patterns made of different concentrations of SA containing PAAm mixtures was dispensed onto the pre-coated hydrophilic/hydrophobic template forming the functional blocks. The functional polymer droplets were allowed to cross-link with the prefabricated thin-film substrate to achieve multipatterned 2D hydrogel complex (Figure 1b). The dispersed PAAm gels with various concentrations of SA are shown in **Table 1**. This method provides a no wash "zero-waste," simple step, and uniform thickness alternative to conventional fabrication methods such as photopolymerization, extrusion, direct ink writing, etc. The multistate 3D shape reconfiguration

Table 1. Composition of high-swelling functional hydrogel patterns and low-swelling nonfunctional substrate thin film.

	Acrylamide [wt%]	Bis-acrylamide [wt%]	TEMED [wt%]	APS [wt%]	SA [wt%]
Pattern I (1B3S)	18.816	3.494	0.168	1.68	16.128
Pattern II (1B1S)	18.816	3.494	0.168	1.69	5.376
Substrate (nonfunctional thin film)	14	0.45	0.35	3.6	0

ADVANCED
SCIENCE NEWS
www.advancedsciencenews.com

ADVANCED
MATERIALS
INTERFACES
www.advmatinterfaces.de

mechanism with maskless swelling/deswelling was then developed and demonstrated (Figure 1c). The number of possible configurations of 3D morphing response to external stimulation can be estimated according to the simple equation,[16] for combined through-thickness and in-plane gradient modes

$$2^n \times 1^m = 2^n \tag{1}$$

where n is associated with the number of in-plan gradient units, while m is associated with the number of through-thickness gradient units. Applied to our proposed structure in Figure 1c, the bilayer gave $m = 2$, and two dissimilar functional blocks on the same plane gave us $n = 2$, which theoretically leads to four possible shape change configurations besides the original state.

2.2. Pre-Gel Droplets Wetting Control in TPP Systems

First, the static CAs of pre-gel droplet on various surfaces were characterized as shown in **Figure 2**a. These CA values were similar to those of deionized (DI) water droplets on the same surfaces. The pre-gel droplet dispensing volume was calculated based on the pattern area (x–y plane in Figure 2b) and the gap distance g. When droplet volumes between the two plates were properly dispensed, the CA θ' (Figure 2c left) remains between 90° and the advancing CA of the hydrogel on the hydrophilic surface (slightly larger than static CA—70° for SiO$_2$). When the volume is slightly larger (Figure 2c right), the gel will still be pinned to the wetting pattern boundary if the θ' lies within the pre-gel advancing CAs on hydrophobic surfaces. The advancing CAs are typically larger than the static CA values as shown in Figure 2a—91°, 109°, and 138° for parylene-C (SCS coatings), perfluorooctyltriethoxysilane (FOTS, Sigma–Aldrich), and Glaco Zero (Soft 99), respectively.

Capillary-driven flow in a TPP system, where the gap height g is significantly smaller than the dimensions of the droplets (Figure 2b,c), the Reynolds number is small enough for us to assume the dynamics can be studied as 2D Hele-Shaw type flow,[34] where the capillary pressure equation can be simplified to

$$P = \kappa_{xy} + \frac{L}{g}\kappa_z \tag{2}$$

where κ_{xy} and κ_z are the nondimensional droplet curvatures in TPP geometry (Figure 2b,c), L is the droplet length scale at x–y plane that is significantly larger than g.

Later work of open microfluidics[35,36] presented the simplified conditions for the liquid to spread along the hydrophilic area/path when flowing such system, summarized by

$$\frac{g}{w} < \frac{\cos\alpha + \cos\theta}{2} \tag{3}$$

where g is the gap between top and bottom plates, w is the width of the droplet wetting front (functional block pattern dimensions in this work) perpendicular to the direction of flow, θ and α are the hydrogel static contact angles (CA) on the top and bottom plates, respectively (Figure 2c). The droplet will stop spreading when the condition set in Equation (2) is not met, e.g., the fluid hits hydrophobic boundary (CA > 90°), and/or the gap g is too large (not in our case as $g \ll w$). Another special consideration is the pre-gel droplet dispensing volume calculation and control. Once the top and bottom plates are in position (g = spacer thickness), a properly controlled dispensing volume should result in a wetting profile as shown in the left-side of Figure 2c. However, if the dispensing volume is too large, resulting the $\theta' >$ advancing CAs on hydrophobic surfaces, the pre-gel solution will de-pin from the boundary, overflowing the patterns and failing the shape control.

Furthermore, due to the relatively small volume changes during this room temperature cross-linking process, nonfunctional substrate wrinkling or bending have not been observed during the functional block polymerization in TPP system.

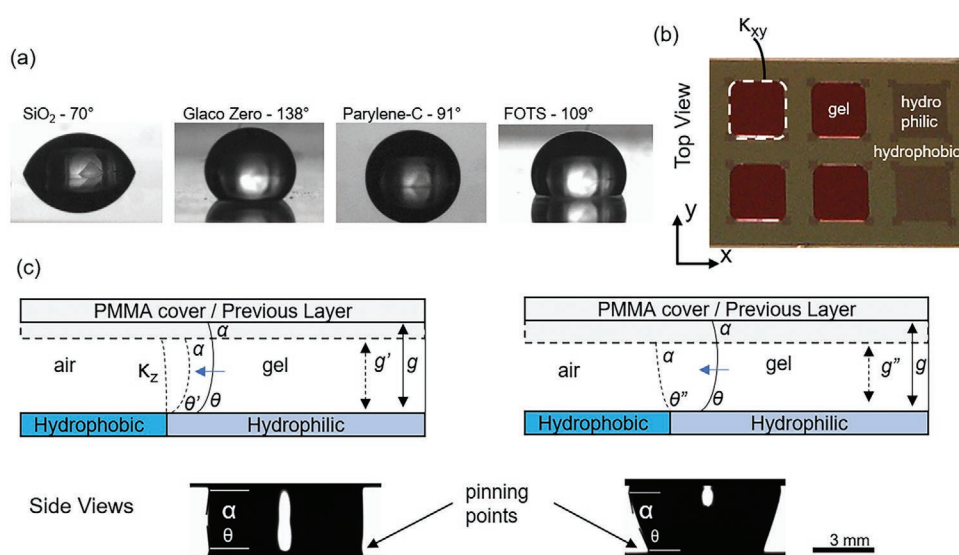**Figure 2.** The wetting behavior of the pre-gel PAAm–SA droplets: a) static CA measurements by DSA; b) top view experimental photograph of the TPP system with pre-gel droplets (red color dye) assembled and shaped by wetting boundaries; c) side view schematic and experimental photograph of the TPP system showing pre-gel droplets spread on hydrophilic patterns and were pinned to the boundaries.

2.3. Hydrogel Mechanical Properties Characterization

To understand the deformation behavior of the heterogeneous hydrogel bilayer structures, mechanical characterization was carried out for functional hydrogel PAAm-SA and the nonfunctional substrate PAAm. Due to its porous structure, mechanical properties such as the Young's modulus for hydrogels change during the swelling process.[37] Hence, an in-house developed "clamp-free" tensile testing platform (**Figure 3**a) was developed to characterize the Young's modulus of both functional and nonfunctional hydrogel systems during the swelling process. The PAAm composites were cast into the desirable shape using a special mold design that directly integrates with the fixing points of the tensile tester as shown by Figure 3a procedure (i) to (iv). Figure 3b shows the strain–stress relationship of the nonfunctional substrate PAAm thin film (Table 1), immersed in 0.2 and 0.5 M PBS solutions for 10 min. The Young's modulus is calculated to be ≈10 and ≈7 kPa for the PAAm film swelled in 0.2 and 0.5 M PBS, respectively. Figure 3c shows the strain–stress relationship of the functional PAAm-SA hydrogel (pattern I—1B3S and pattern II—1B1S in Table 1). It can be clearly seen that the higher PBS concentration resulted in higher Young's modulus in all cases. We attribute this behavior to highly crystalline nature of the hydrogel molecules reducing the interface defects in the crystalline region and the amorphous area making the elongation longer. The modulus value of the PAAm thin film also matches those reported by Denisin and Pruitt,[38] which was set as a benchmark.

The swelling and deswelling ratios dynamically responding to PBS concentration (0–0.5 M) and SA compositions were obtained. In our previous PAAm-SA (different composition)

swelling study,[39] various boundary confinement conditions were characterized—freestanding, one-side confinement, and ring confinement. In this work, the 3D morphing bilayer structure was placed in "freestand" mode in PBS/water solutions and the swelling ratio characterizations of PAAm and PAAm-SA hydrogel spheres were conducted (**Figure 4**a). The swelling ratio was given by

$$\text{Swelling ratio} = \frac{d_{swell}}{d_{origin}} \qquad (4)$$

Figure 4b–d shows the swelling ratios of all three PAAm-SA and PAAm compositions (Table 1) over time, in DI water, 0.2 M PBS, and 0.5 M PBS, respectively. The PAAm nonfunctional substrate did not exhibit significant swelling or deswelling behavior, with its diameter topped by 119% of its original value at the end of the tests. For PAAm-SA pattern I (1B3S in Table 1) and pattern II (1B1S in Table 1), significant swelling (up to 275%) and deswelling (down to 2%) occurred when immersed in DI water (Figure 4b) and 0.5 M PBS (Figure 4d), respectively. Figure 4c shows the interesting observation that when both PAAm-SA composites were immersed in 0.2 M PBS, the pattern I (1B3S) swells significantly to 241% of its original diameter, while to the opposite pattern II (1B1S) deswells significantly to 2% of its original diameter. This large dissimilarity can potentially result in huge deformation magnitudes.

Due to the high aspect ratio (g << w, Section 2.2) of the TPP molding system, the functional blocks have a large surface area to thickness ratio, compared with the spheres used in swelling test shown in Figure 4. This has successfully accelerated the reaction time of the transducers with typical an onset of shape
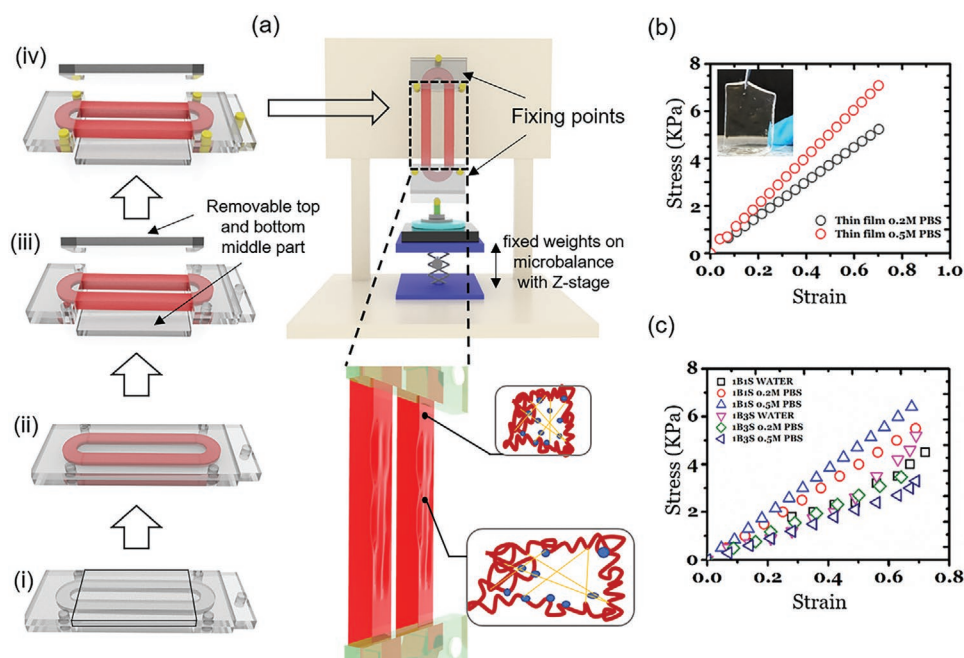
Figure 3. Mechanical property characterization a) in-house developed clamp-free tensile tester for swelling hydrogels, with procedures (i) to (iv) showing the molding setup where as-fabricated PAAm composites can be directly integrated with the tensile tester; b,c) strain–stress relationship of b) the nonfunctional substrate PAAm thin film, immersed in 0.2 and 0.5 M PBS solutions for 10 min; and c) the functional PAAm–SA immersed in DI water, 0.2 and 0.5 M PBS solutions for 10 min.

**ADVANCED
SCIENCE NEWS**

www.advancedsciencenews.com

**ADVANCED
MATERIALS
INTERFACES**

www.advmatinterfaces.de

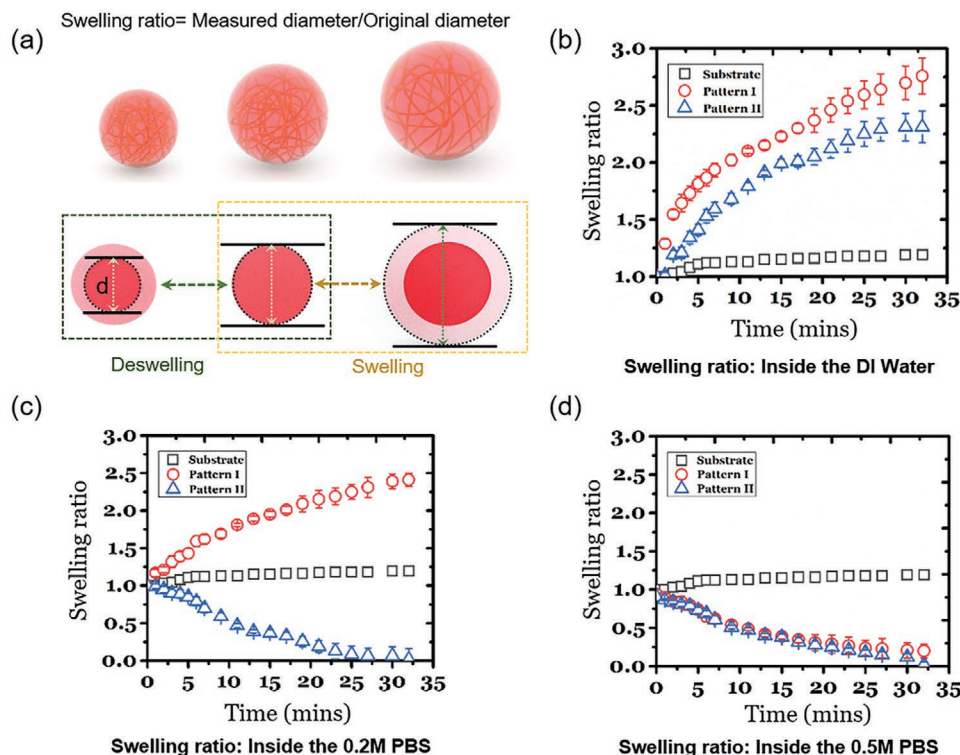**Figure 4.** a) Swelling ratio characterization using freestanding hydrogel spheres. b–d) Swelling ratio versus time—for nonfunctional substrate (PAAm), and patterns I and II (PAAm-SA) samples immersed in b) DI water; c) 0.2 M PBS; and d) 0.5 M PBS.

morphing occurring around 2 min of immersion, which was determined by the swelling and deswelling characteristics of the thin functional blocks.

2.4. Numerical Modeling of the Reconfigurable Deformation

Based on the mechanical characterization results obtained, numerical modeling was conducted to help design/programme the morphing configurations under certain external stimulation. Meanwhile the reconfigurability of the same bilayer heterogeneous structure was also studied.

The deformation process of the heterogeneous gel structure is simulated by solving the following mechanical equilibrium equation

$$\nabla \cdot \underline{S} = 0 \tag{5}$$

where $\underline{S}$ is the nominal stress tensor and ∇ is the operator of divergence with respect to the reference state, i.e., the initial state of the gel without swelling or deswelling. Details of the simulation are included in the Supporting Information.

The in-plane gradient gel structure composed of only two functional blocks can exhibit three different configurations, i.e., straight (nonactivated), "S", "C", and "W" shapes as shown in **Figure 5**. When the functional gel block expands (swells), it will induce an internal tensile stress (σ) on the top surface of the nonfunctional substrate, which will generate a clockwise bending moment (M) and bend the unit to a convex configuration (Figure 5a). On the other hand, the contracting (deswelling) gel block induces an internal compressive stress
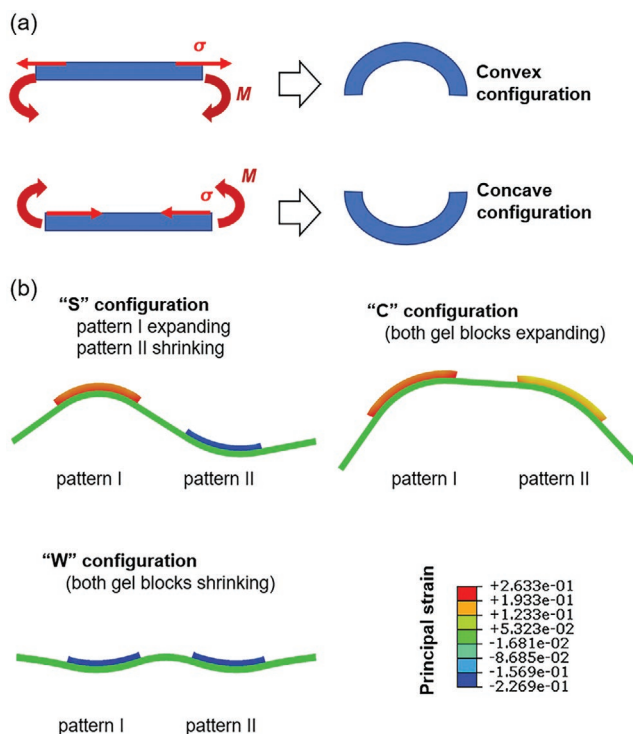

Figure 5. Mechanical model of the reconfigurable deformation: a) convex and concave configuration due to bending moment; b) numerical simulation results showing three different configurations induced by swelling and deswelling of patterns I and II, based on the obtained mechanical property and swelling ratio results.

2001211 (5 of 8)

on the top surface of the substrate, which will bend the unit to a concave configuration due to the generated counterclockwise bending moment (Figure 5a). The radius R of curvature of the unit depends on the swelling ratio ρ of the gel, and the thicknesses of the gel (t_g) and the substrate (t_s). Then by scaling analysis, we have

$$\frac{R}{t_g} = f\left(\rho, \frac{t_s}{t_g}\right) \quad (6)$$

In the simplest case where both the gel block and the substrate are homogeneous and the unit is simplified as Euler–Bernoulli beam, we can further approximate the scaling as

$$\frac{R}{t_g} = -\frac{t_s/t_g}{2(\rho - 1)} \quad (7)$$

where $R < 0$ corresponds to convex configuration and $R > 0$ corresponds to concave one.

Figure 5b shows the three different cases (reconfigurable states), programmed with two dissimilar functional gel blocks responding to external ion concentration. In the first case where the left gel block (pattern I) expands (swells) and the right one (pattern II) contracts (deswells), the left unit bends to a convex configuration while the right unit bends to a concave one, which leads to an "S" shape of the structure. In the second case, both gel blocks expand, so the two units bend to convex configurations, which make the total structure exhibit a "C" shape. In the third case, both gel blocks contract and the units bend to concave configurations, leading to a "W" shape.

The in-plane gradient gel structure of two different functional blocks is the basic element. By combining more elements, structures exhibiting more complex 3D configurations/shapes can be obtained. Figure S2a, Supporting Information, shows an example of a structure combining three elements that can exhibit a complex 3D wavy configuration.

2.5. Reconfigurable Multistate 3D Morphing Demonstration

The localized swelling and deswelling characteristics of the patterned gels and resulting configurations imparted onto the nonfunctional substrate are closely related to the ionic concentration of the environment. The patterned gel's periodicity can be tuned by adding more hydrophilic features onto the hydrophobic polyacrylic plate. Selective dispensing of functional gels with distinctive SA magnitude results in localized spatial configuration that is switchable under different ionic environment (**Figure 6**). As shown in Figure 6a, both the low (pattern II) and high concentration (pattern I) SA functional blocks swell in DI water at alternative rate due to ionic equilibrium and thus forming a concave shape of the nonfunctional layer. At 0.2 M PBS, due to the osmotic imbalance, high concentration SA patterned functional block undergoes a positive swelling leading to upward buckling of the nonfunctional substrate. Whereas, the low concentration SA functional block undergoes negative swelling leading to downward buckling resulting in a "S"-shaped configuration (Figure 6b). At 0.5 M PBS, due to increase in PBS concentration, both the functional groups undergo deswelling forming a "W"-shaped configuration that matches our theoretical simulation results (Figures 5b and 6c). We believe, the buckling conformation is achieved due to the influence of high transient swelling forces with swelling mismatch occurring in one of the functional blocks.[40] When more than two patterns were involved, complex surface convex and concave buckling can be observed that transients over time
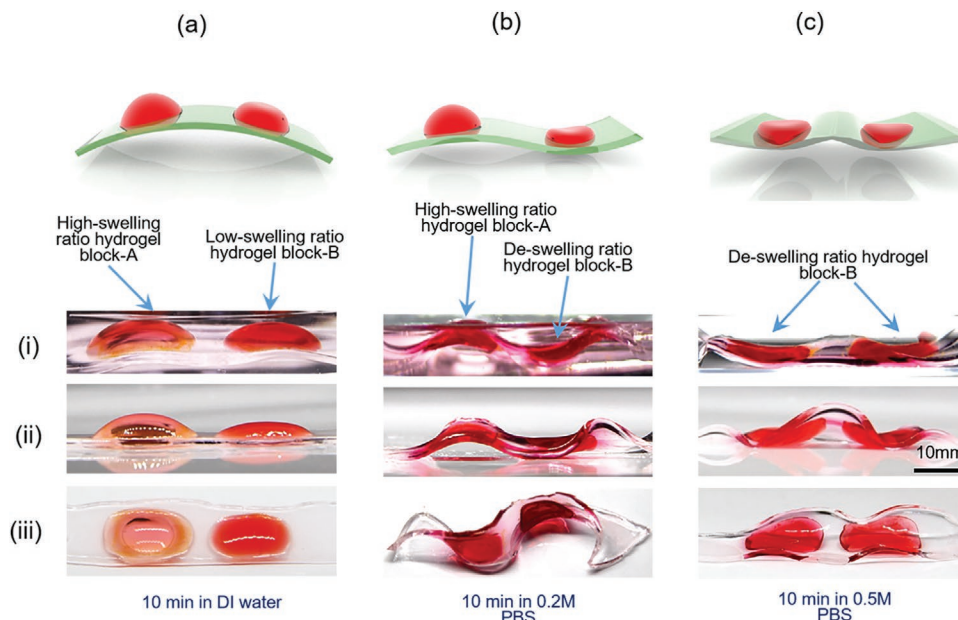

Figure 6. Representative complex 3D conformable configurations with mask-free swelling/deswelling, deformed from 2D patterned functional/nonfunctional hydrogels ionic imbalance. a) Concave deformation achieved by immersing the transducers in DI water. b) Buckling mismatch configuration of hydrogel transducer in 0.2 M PBS. c) Cooperative deswelling of both high and low SA patterns in 0.5 M PBS. Rows (i) to (iii) represent different viewing angles and condition: i) Structure in solution—side view; ii) structure in air (gravity in play)—side view; and iii) structure in air—top view.

**ADVANCED
SCIENCE NEWS**
www.advancedsciencenews.com

**ADVANCED
MATERIALS
INTERFACES**
www.advmatinterfaces.de

with changing diffusion coefficients and ionic equilibrium, as detailed in the Supporting Information and Figure S2, Supporting Information.

3. Conclusion

Reconfigurable multistate 3D morphing has been achieved through PAAm/PAAm-SA hydrogel bilayer structure that was created in a "TPP" (Hele-Shaw cell) open-microfluidic configuration. The mechanical characterization was carried out to understand the gel property change during the swelling and deswelling processes. The numerical analysis was performed to help understand the morphing states and swelling configurations, which agrees with the experimental observation. The gel structure switching between three different morphing configurations was demonstrated, driven by in-plane and through-thickness heterogeneity during stimuli-responsive swelling subject to ionic concentration change.

Since the PAAm-based hydrogel can potentially be engineered to respond to various inputs (e.g., temperature, light, electrical field, magnetic field), we anticipate such heterogeneous multilayered structures will unlock more advances in the morphing soft transducer applications. For example, a triple-layered (or more) heterogeneous structure exhibiting a dual responsive thermoelectric behaviour can be manufactured to display multiplexed in/output configurations. On the other hand, the reconfigurable morphing structure could also be employed for topography-induced actuations such as complex topo-optical pattern generation.[41] They can also be attached as a replacement for conventional metallic electrodes, organic electrochemical transistors, with tuneable geometry/curvature to be conformal with complex biological surface topography.

Furthermore, the wetting-enabled gel assembly and shape-controlled gelation process in TPP systems could potentially be scaled up/down, inspired by existing printing technologies such as ODF (one droplet filling) employed in liquid crystal display manufacturing. During the ODF process, droplets (e.g., liquid crystal) are dispensed into physically closed/confined cells. Further study will be required to adopt this technology in open-microfluidics configurations.

4. Experimental Section

Hydrogel Bilayer Preparation: The high-swelling functional hydrogel patterns I and II were created from PAAm network with SA that contains free positive sodium ions. *N,N′*-Methylenebisacrylamide (BisAA or MBAA) was used as a cross-linker, with *N,N,N′,N′*-tetramethylethylenediamine (TEMED) and ammonium persulfate (APS) used as initiators for the polymerization process.

Surface Treatment of TPP Open Microfluidics: The TPP system consists of a hydrophobically treated poly(methyl methacrylate) (PMMA) acrylic top plate, and a bottom plate (35 × 80 mm rectangle chip cut from polished silicon wafers) with hydrophobic/hydrophilic wetting control patterns. The hydrophilic zone on the bottom plate was 1 μm thermally oxidized SiO_2 layer. And three different types of hydrophobic coating materials were used: spray-coated Glaco Mirro Zero (Soft99), vapor-coated parylene-C (SCS coatings), and FOTS (Sigma–Aldrich). The patterning was done via shadow masking (Glaco Zero and FOTS), or photolithography followed by oxygen plasma etching (parylene-C).

Hydrogel Bilayer Patterning Using TPP Open Microfluidics: A detailed recipe of the functional/nonfunctional substrates is listed in Table 1. A 2.5mL of nonfunctional PAAm solution was dispensed onto the hydrophobic/hydrophilic bottom plate with a defined gap size and gelled to form a thin film (Figure 1a). This was followed by 40 μL of PAAm solution with varied SA concentration dispensed onto another prefabricated hydrophobic/hydrophilic patterned plate with a spacer to adjust the overall thickness of the functional patterns (Figure 1a). For pattern transfer, the PMMA plate containing nonfunctional thin film was placed over the multipatterned functional gels and allowed to cross-link. Afterwards, to achieve multiconfigurable 3D shape-morphing states, the patterned nonfunctional substrate was allowed to freestand in different ionic concentrations of PBS and water for 10 min. The pre-gel solutions were dispensed to polymerize and shaped inside a Hele-Shaw cell (TPP) layered by hydrophobic and hydrophilic boundaries inside the TPP system before polymerization.

Hydrogel Wetting Characterization: The static CA measurement was performed on Kruss DSA30S system. The pre-gel samples were mixed and measured within 15 min of preparation. The droplet volumes were kept at 5 μL each, manually dispensed on leveled surfaces with different coatings. The results are presented in Figure 2a.

TPP System Setup: The construction of the Hele-Shaw cell system is similar to that presented by Walton and co-workers,[42,43] where spacing materials (e.g., plastic shims with thickness range 0.025–3 mm) were used as spacers to control the gap height. First, the pre-gel of the nonfunctional hydrogel substrate—a fine volume controlled low-swelling hydrogel—was micropipetted within the hydrophilic zone of the bottom plate surface. The PMMA top plate was then lowered towards the bottom plate, leaving a small gap g in between. The pre-gel was shaped following the hydrophobic/hydrophilic boundary, with its thickness = g. The wetting and gelation process observation of the TPP system is explained in the Supporting Information (Figure S1, Supporting Information).

Supporting Information

Supporting Information is available from the Wiley Online Library or from the author.

Conflict of Interest

The authors declare no conflict of interest.

[1] S. Armon, E. Efrati, R. Kupferman, E. Sharon, *Science* **2011**, *333*, 1726.

[2] I. W. Hamley, V. Castelletto, *Angew. Chem., Int. Ed.* **2007**, *46*, 4442.

[3] S. Li, H. Bai, R. F. Shepherd, H. Zhao, *Angew. Chem., Int. Ed.* **2019**, *58*, 11182.

[4] Y. Liu, J. Genzer, M. D. Dickey, *Prog. Polym. Sci.* **2016**, *52*, 79.

[5] L. Ionov, *Adv. Funct. Mater.* **2013**, *23*, 4555.

[6] X. Liu, J. Liu, S. Lin, X. Zhao, *Mater. Today* **2020**, *36*, 102.

[7] F. G. Downs, D. J. Lunn, M. J. Booth, J. B. Sauer, W. J. Ramsay, R. G. Klemperer, C. J. Hawker, H. Bayley, *Nat. Chem.* **2020**, *12*, 363.

[8] A. Cangialosi, C. Yoon, J. Liu, Q. Huang, J. Guo, T. D. Nguyen, D. H. Gracias, R. Schulman, *Science* **2017**, *357*, 1126.

[9] J. Zhao, U. Gulan, T. Horie, N. Ohmura, J. Han, C. Yang, J. Kong, S. Wang, B. B. Xu, *Small* **2019**, *15*, 1900019.

[10] K.-I. Jang, K. Li, H. U. Chung, S. Xu, H. N. Jung, Y. Yang, J. W. Kwak, H. H. Jung, J. Song, C. Yang, A. Wang, Z. Liu, J. Y. Lee, B. H. Kim, J.-H. Kim, J. Lee, Y. Yu, B. J. Kim, H. Jang, K. J. Yu, J. Kim, J. W. Lee, J.-W. Jeong, Y. M. Song, Y. Huang, Y. Zhang, J. A. Rogers, *Nat. Commun.* **2017**, *8*, 15894.

[11] H. Fu, K. Nan, W. Bai, W. Huang, K. Bai, L. Lu, C. Zhou, Y. Liu, F. Liu, J. Wang, M. Han, Z. Yan, H. Luan, Y. Zhang, Y. Zhang, J. Zhao, X. Cheng, M. Li, J. W. Lee, Y. Liu, D. Fang, X. Li, Y. Huang, Y. Zhang, J. A. Rogers, *Nat. Mater.* **2018**, *17*, 268.

[12] C. A. Spiegel, M. Hippler, A. Münchinger, M. Bastmeyer, C. Barner-Kowollik, M. Wegener, E. Blasco, *Adv. Funct. Mater.* **2020**, *30*, 1907615.

[13] S. Naficy, R. Gately, R. Gorkin III, H. Xin, G. M. Spinks, *Macromol. Mater. Eng.* **2017**, *302*, 1600212.

[14] A. Kirillova, L. Ionov, *J. Mater. Chem. B* **2019**, *7*, 1597.

[15] B. J. Cafferty, V. E. Campbell, P. Rothemund, D. J. Preston, A. Ainla, N. Fulleringer, A. C. Diaz, A. E. Fuentes, D. Sameoto, J. A. Lewis, G. M. Whitesides, *Adv. Mater. Technol.* **2019**, *4*, 1800299.

[16] C. Y. Li, X. P. Hao, S. Y. Zheng, W. Hong, Q. Zheng, Z. L. Wu, *Adv. Intell. Syst.* **2019**, *1*, 1900055.

[17] Z. J. Wang, W. Hong, Z. L. Wu, Q. Zheng, *Angew. Chem., Int. Ed. Engl.* **2017**, *56*, 15974.

[18] X. P. Hao, Z. Xu, C. Y. Li, W. Hong, Q. Zheng, Z. L. Wu, *Adv. Mater.* **2020**, *32*, 2000781.

[19] Z. J. Wang, C. Y. Li, X. Y. Zhao, Z. L. Wu, Q. Zheng, *J. Mater. Chem. B* **2019**, *7*, 1674.

[20] Y. Zhou, C. M. Duque, C. D. Santangelo, R. C. Hayward, *Adv. Funct. Mater.* **2019**, *29*, 1905273.

[21] C. Y. Li, X. P. Hao, Z. L. Wu, Q. Zheng, *Chem. - Asian J.* **2019**, *14*, 94.

[22] X. Zhou, T. Li, J. Wang, F. Chen, D. Zhou, Q. Liu, B. Li, J. Cheng, X. Zhou, B. Zheng, *ACS Appl. Mater. Interfaces* **2018**, *10*, 9077.

[23] S. Y. Zheng, Y. Shen, F. Zhu, J. Yin, J. Qian, J. Fu, Z. L. Wu, Q. Zheng, *Adv. Funct. Mater.* **2018**, *28*, 1803366.

[24] G. Gao, Z. Wang, D. Xu, L. Wang, T. Xu, H. Zhang, J. Chen, J. Fu, *ACS Appl. Mater. Interfaces* **2018**, *10*, 41724.

[25] B. Xu, R. C. Hayward, *Adv. Mater.* **2013**, *25*, 5555.

[26] B. B. Xu, Q. Liu, Z. Suo, R. C. Hayward, *Adv. Funct. Mater.* **2016**, *26*, 3218.

[27] Z. J. Wang, C. N. Zhu, W. Hong, Z. L. Wu, Q. Zheng, *Sci. Adv.* **2017**, *3*, e1700348.

[28] R. M. Erb, J. S. Sander, R. Grisch, A. R. Studart, *Nat. Commun.* **2013**, *4*, 1712.

[29] Y. Zhang, X. Le, Y. Jian, W. Lu, J. Zhang, T. Chen, *Adv. Funct. Mater.* **2019**, *29*, 1905514.

[30] S. Park, D. Kim, S. Y. Ko, J.-O. Park, S. Akella, B. Xu, Y. Zhang, S. Fraden, *Lab Chip* **2014**, *14*, 1551.

[31] M.-Y. Chiang, Y.-W. Hsu, H.-Y. Hsieh, S.-Y. Chen, S.-K. Fan, *Sci. Adv.* **2016**, *2*, e1600964.

[32] C. Wang, S. Sridhar, J. G. Terry, A. Sun, Z. Li, H. Lv, B. B. Xu, Y. Li, presented at 2019 20th Int. Conf. on Solid-State Sensors, Actuators and Microsystems & Eurosensors XXXIII (TRANSDUCERS & EUROSENSORS XXXIII), Berlin, Germany, June 2019.

[33] E. E. Charrier, K. Pogoda, R. Li, C. Y. Park, J. J. Fredberg, P. A. Janmey, *APL Bioeng.* **2020**, *4*, 036104.

[34] S. W. Walker, B. Shapiro, *J. Microelectromech. Syst.* **2006**, *15*, 986.

[35] U. N. Lee, J. H. Day, A. J. Haack, R. C. Bretherton, W. Lu, C. A. DeForest, A. B. Theberge, E. Berthier, *Lab Chip* **2020**, *20*, 525.

[36] B. P. Casavant, E. Berthier, A. B. Theberge, J. Berthier, S. I. Montanez-Sauri, L. L. Bischel, K. Brakke, C. J. Hedman, W. Bushman, N. P. Keller, D. J. Beebe, *Proc. Natl. Acad. Sci. USA* **2013**, *110*, 10111.

[37] J. Macron, A. P. Gerratt, S. P. Lacour, *Adv. Mater. Technol.* **2019**, *4*, 1900331.

[38] A. K. Denisin, B. L. Pruitt, *ACS Appl. Mater. Interfaces* **2016**, *8*, 21893.

[39] Y. Li, D. Wang, J. Richardson, B. B. Xu, *Macromol. Symp.* **2017**, *372*, 127.

[40] A. Ilseng, V. Prot, B. H. Skallerud, B. T. Stokke, *J. Mech. Phys. Solids* **2019**, *128*, 219.

[41] C. Wang, D. Wang, V. Kozhevnikov, X. Dai, G. Turnbull, X. Chen, J. Kong, B. Z. Tang, Y. Li, B. B. Xu, *Nat. Commun.* **2020**, *11*, 1448.

[42] I. Schmueser, E. O. Blair, Z. Isiksacan, Y. Li, D. K. Corrigan, A. A. Stokes, J. G. Terry, A. R. Mount, A. J. Walton, presented at 2020 IEEE 33rd Int. Conf. on Microelectronic Test Structures (ICMTS), May 2020.

[43] Y. Li, E. O. McKenna, W. Parkes, A. R. Pitt, A. J. Walton, *Appl. Phys. Lett.* **2011**, *99*, 073703.